Coupled electronic and nuclear dynamics at interfaces of artificial photosynthesis devices

Haas, T. de

Chapter 2: Theory and Methodology

Molecular simulation methods rely on a broad array of approximations to efficiently describe the dynamics of nuclei and electrons. This chapter provides a brief outline of the methods relevant for this dissertation and discusses advantages and disadvantages of each method.

2.1 Introduction

The work described in this dissertation hinges on a simple, yet powerful concept: that the complex behavior of a system of interest can be studied by applying the laws of physics on a representative model. This implies that the dynamical behavior and photochemical response of molecules and materials can be predicted from their elementary structure by applying the laws of quantum mechanics. Unfortunately, the quantum mechanical calculations resulting from those laws are associated with a numerical cost that scales exponentially with the system size. Quantum computers hold promise to crack this exponential scaling problem, but for now their hardware is insufficiently developed to be practically useful. Therefore, modern quantum chemistry still relies on a broad range of approximations, and the difficulty in this field often lies in finding a workable compromise between computational efficiency and accuracy.

This chapter provides an introduction into the conceptual frameworks used in this dissertation for studying a range of molecular phenomena. Section 2.2 deals with the quantum-mechanical laws of physics that describe the behavior of electrons and atomic nuclei. Application of these laws results in a recipe to calculate interatomic forces, which can be used to study the dynamics of molecular systems as well as bond formation and breaking. Section 2.3 concentrates on how the equations of motion can be integrated over time, yielding a description of molecular dynamics in the ground state. In Section 2.4, the discourse extends to an electronic excited state situation, which is crucial for capturing the physics of light-induced processes. Section 2.5 deals with extracting thermodynamic properties from molecules in their minimum energy structure. The final section 2.6 goes more in-depth on the electronic structure methods used in this work.

2.2 Electronic structure theory and the Born-Oppenheimer approximation

In this chapter, we assume that the physics relevant for chemistry is described by the non-relativistic, time-dependent Schrödinger equation, which in atomic units ($\hbar = m_\mathrm{e} = 4\pi\epsilon_0 = e = 1$) takes the form:

$$\hat{H}\,\Phi(\boldsymbol{r},\boldsymbol{R},t) = i\frac{\partial}{\partial t}\Phi(\boldsymbol{r},\boldsymbol{R},t) \tag{2.1}$$

where i is the imaginary unit, Φ represents a wavefunction that depends on time t and on both electronic coordinates $\boldsymbol{r}$ and nuclear coordinates $\boldsymbol{R}$, and $\hat{H}$ is the Hamiltonian describing the system. Note that throughout this dissertation, vectors and matrices are written in bold, and operators are written with a circonflexe ("little hat"). $\boldsymbol{r}$ and $\boldsymbol{R}$ thus represent a column vector containing all electronic and nuclear positions, respectively. For chemical purposes, it is sufficient to model the atomic nucleus as a point charge Z_I located at the position $\boldsymbol{R}_I$. The Hamiltonian for a chemical system with N nuclei and n electrons is thus given by:

Here, M_I and m_i represent the nuclear and electronic masses, respectively. In this

$$\hat{H} = -\sum_{I=1}^{N}\frac{1}{2M_I}\nabla_{R_I}^2 - \sum_{i=1}^{n}\frac{1}{2m_i}\nabla_\mathrm{r}^2 + \left[\sum_{i<j}^{n}\frac{1}{|\boldsymbol{r}_i - \boldsymbol{r}_j|} - \sum_{I,i}^{N,n}\frac{Z_I}{|\boldsymbol{R}_I - \boldsymbol{r}_i|} + \sum_{I<J}^{N}\frac{Z_I Z_J}{|\boldsymbol{R}_I - \boldsymbol{R}_J|}\right]. \tag{2.2}$$

equation, we can identify in order, the kinetic energy operator for the nuclei, the kinetic energy operator for the electrons and the Coulomb operators for the electron-electron, electron-nuclei and nuclei-nuclei interactions. It is useful to regroup these terms into an electronic Hamiltonian, $\hat{H}_\mathrm{e}$, and a nuclear Hamiltonian, $\hat{H}_\mathrm{n}$. By convention, this separation is defined such that the nuclear Hamiltonian contains the nuclear kinetic energy operator, while the electronic Hamiltonian contains all the other terms:

$$\hat{H} = -\sum_{I=1}^{N}\frac{1}{2M_I}\nabla_{R_I}^2 + \hat{H}_\mathrm{e} \tag{2.3}$$

Using the electronic Hamiltonian, we can also define the electronic wavefunctions $\Psi_i(\boldsymbol{r};\ \boldsymbol{R})$ as the set of functions that satisfy the following eigenvalue problem, also known as the time-independent electronic Schrödinger equation:

$$\hat{H}_{\mathrm{e}}\Psi_i(\boldsymbol{r};\ \boldsymbol{R}) = E_i\Psi_i(\boldsymbol{r};\ \boldsymbol{R})\,. \tag{2.4}$$

The eigenfunctions $\Psi_i(\boldsymbol{r};\ \boldsymbol{R})$ form a complete and orthonormal basis, in which the nuclear dependence is included parametrically. This is convenient because most chemical calculations do not require a full quantum-mechanical description of both nuclei and electrons.

In the work presented in this thesis, the electronic system is treated quantum mechanically, while the atomic nuclei are treated classically. This is generally justifiable, as quantum effects become less prominent for heavier particles. To show that a mixed quantum-classical description can be derived neatly from the above equations, we follow a route proposed by Doltsinis and Marx.[1] This route also sets up the framework of equations from which we can later derive the surface hopping algorithm proposed by Tully.[2] The following multiconfigurational ansatz for the wavefunction is proposed:

$$\Phi(\boldsymbol{r},\boldsymbol{R},t) = \sum_j^{\infty} \Psi_j(\boldsymbol{r};\ \boldsymbol{R})\, X_j(\boldsymbol{R},t)\,. \tag{2.5}$$

This ansatz separates the total wavefunction $\Phi(\boldsymbol{r},\boldsymbol{R},t)$ into an electronic part, $\Psi_j(\boldsymbol{r};\ \boldsymbol{R})$, and a nuclear part, $X_j(\boldsymbol{R},t)$. The subscript j runs over the electronic basis functions, effectively associating to each electronic basis state a nuclear wavefunction. The solutions to equation (2.4) present a convenient basis for the electronic wavefunction. The nuclear wavefunctions do not need to be orthogonal or normalized. When equation (2.5) is inserted into equation (2.1) we can derive an expression for the time-evolution of $X_i(\boldsymbol{R},t)$. By inserting the ansatz, multiplying from the left with $\Psi_i^*(\boldsymbol{r};\boldsymbol{R})$, and subsequently integrating over $\boldsymbol{r}$, the following equation is obtained for the time-evolution of the nuclei:

$$i\,\frac{\partial X_j(\boldsymbol{R},t)}{\partial t} = \left[-\sum_{I=1}^{N}\frac{1}{2M_I}\nabla_{R_I}^2 + E_j\,(\boldsymbol{R})\right]X_j(\boldsymbol{R},t) + \sum_{i}^{\infty}\left[\sum_{I}^{N}\frac{1}{2M_I}D_{ji}^I - \sum_{I}^{N}\frac{1}{M_I}d_{ji}^I\nabla_{R_I}\right]X_i(\boldsymbol{R},t) \qquad (2.6)$$

Note that, subscript i and j run over the electronic state indexes, while I runs over the nuclear particle indexes. E_j represents the matrix element $\langle\Psi_j(\boldsymbol{r};\,\boldsymbol{R})|\hat{H}_{\mathrm{e}}|\Psi_j(\boldsymbol{r};\,\boldsymbol{R})\rangle$ while d_{ji}^I and D_{ji}^I represent the first and second order non-adiabatic coupling terms, given by:

$$d_{ji}^I = \langle\Psi_j(\boldsymbol{r},\boldsymbol{R})|\nabla_{R_I}|\Psi_i(\boldsymbol{r},\boldsymbol{R})\rangle \qquad (2.7)$$

and

$$D_{ji}^I = \langle\Psi_j(\boldsymbol{r},\boldsymbol{R})|\nabla_{R_I}^2|\Psi_i(\boldsymbol{r},\boldsymbol{R})\rangle \qquad (2.8)$$

The bra-ket notation signifies an integral over the space of all electronic coordinates.[3] We can simplify equation (2.6) considerably by invoking the adiabatic approximation, which neglects all the non-diagonal terms in d_{ji}^I and all the second order terms D_{ji}^I:

$$i\,\frac{\partial X_j(\boldsymbol{R},t)}{\partial t} = \left[-\sum_{I=1}^{N}\frac{1}{2M_I}\nabla_{R_I}^2 + E_j\,(\boldsymbol{R}) + \sum_{I=1}^{N}\frac{1}{2M_I}d_{jj}^I\right]X_j(\boldsymbol{R},t) \qquad (2.9)$$

The Born-Oppenheimer approximation is now recovered by neglecting also the diagonal terms d_{jj}^I:

$$i\,\frac{\partial X_j(\boldsymbol{R},t)}{\partial t} = \left[-\sum_{I=1}^{N}\frac{1}{2M_I}\nabla_{R_I}^2 + E_j\,(\boldsymbol{R})\right]X_j(\boldsymbol{R},t) \qquad (2.10)$$

This equation evolves the nuclear wavefunction in an average potential generated by the electronic sub-system, which is quenched to a specific eigenstate of the electronic Hamiltonian E_j. Despite invoking several approximations, equation (2.10) remains prohibitively expensive to solve numerically for most problems

encountered in chemistry. However, as stated before, in most cases it is reasonable to describe the nuclear motion classically. By assuming classical behavior of the atomic nuclei, equation (2.10) can be rewritten[1] to yield Newtons equations of motion for the classic nuclei evolving in a quantum mechanical potential generated by the electrons:

$$M_I \frac{d^2}{dt^2} \boldsymbol{R}_I(t) = -\nabla_I E_j(\boldsymbol{R}) = \boldsymbol{F}_I(t) \tag{2.11}$$

Here, E_j is found by solving the eigenvalue equation (2.4). Typically, we are interested in the behavior of a system in the electronic ground state, where *j*=0. Equation (2.11) demonstrates that the time-evolution of the nuclear positions $\boldsymbol{R}_I$ can be computed using only the gradient of the electronic energy with respect to the nuclei $\nabla_I E_j(\boldsymbol{R})$. The next section will focus on integrating these equations of motion in an efficient manner.

2.3 Molecular Dynamics and Thermodynamics

One of the most popular algorithms to numerically integrate equations (2.11) is the Velocity Verlet algorithm.[4] Since the computation of equation (2.4) depends only on the nuclear positions and not on the velocities, the algorithm can be divided in an initation step followed by a 5 step cycle according to:

1. Initiate the system at t_0 by providing an initial set of nuclear positions $\boldsymbol{R}_I(t)$ and velocities $\boldsymbol{v}_I(t)$, and calculate the accelerations $\boldsymbol{a}_I(t)$ from equation (2.11) as $\boldsymbol{F}_I(t)/M_I$.
2. Calculate the new positions:

   $$\boldsymbol{R}_I(t + \Delta t) = \boldsymbol{R}_I(t) + \boldsymbol{v}_I(t)\Delta t + \frac{1}{2}\,\boldsymbol{a}_I(t)\Delta t^2$$

3. With the newly obtained set of positions compute the accelerations at the next time step $\boldsymbol{a}_I(t + \Delta t)$.
4. Calculate the new velocities:

   $$\boldsymbol{v}_I(t + \Delta t) = \boldsymbol{v}_I(t) + \frac{1}{2}\left(\boldsymbol{a}_I(t) + \boldsymbol{a}_I(t + \Delta t)\right)\Delta t$$

5. Set the current time step t to the new time step $t + \Delta t$.
6. If the simulation time exceeds the desired simulation time t_{final}, terminate the simulation. Otherwise, go back to step 2.

After initialization, this algorithm iteratively computes the nuclear positions $\boldsymbol{R}_I(t + \Delta t)$ at the next time step, $t + \Delta t$, from the nuclear velocities and accelerations at the current time t, until the total simulation time reaches a satisfactory length. Due to its third order numerical precision in Δt and low memory intensity, this algorithm has become the default molecular dynamics (MD) propagator in state-of-the-art computational chemistry codes. A critical parameter for any integration scheme is the time step Δt, which is chosen such that the total energy, *i.e.* the combination of the potential and the kinetic energy in the simulation is conserved. Typically, this means that the shortest oscillation period in the system of interest is described with *ca.* 10 time steps. For a molecular system in the ground state, these oscillations are the vibrations of C-H or O-H bonds, whose characteristic stretching frequencies are properly described with a time step of 0.5 fs. If the time-evolution of the electronic subsystem is considered explicitly, a much shorter time step of 0.01 fs is generally required.[5]

Despite the numerical robustness of the Velocity Verlet Algorithm, tracing the exact trajectory of a molecular system on longer timescales is impossible. Fortunately, we are interested in the collective properties of a molecular ensemble rather than the precise dynamics of an individual molecule. The basic assumption underpinning all MD simulations is that the ensemble average of an observable in a macroscopic system is equivalent to the time average of this observable in a microscopic system.

The most straightforward way to perform a MD simulation, is to initialize a predefined number of particles in a box with fixed dimensions and start integrating the equations (2.11). Such a simulation at constant volume (*V*), constant particle number (*N*), and constant total energy (*E*) of the system, reproduces the *NVE* ensemble or microcanonical ensemble. Often, one would like to sample an

ensemble at thermal equilibrium with an external heat bath, to mimic experimental conditions. This ensemble is referred to as the *NVT* or canonical ensemble. To achieve this desired phase space distribution, a range of different thermostats have been developed which all try to obey physical constraints such as microscopic reversibility and continuous trajectories without requiring a large computational overhead. Notable examples of commonly applied thermostats are the Nose-Hoover Chain and the Canonical Sampling through Velocity Rescaling thermostats.[6–8] Besides temperature constraints, performing dynamics simulations at constant pressure by changing the box volume can often be useful. Such isoenthalpic-isobaric (*NPH*) or isothermal-isobaric (*NPT*) simulations can be used to achieve a realistic density of molecules in the simulation. Finally, for chemical purposes it is useful to define the grand canonical ensemble with constant chemical potential (μ), volume (V) and temperature (T).

All statistical ensembles are associated with an intrinsic thermodynamic potential, which measures the internal energy change when the system evolves from one microstate to the other. For the *NVT* ensemble, this property is called the Helmholtz free energy, *F*, which is defined as:

$$F \equiv U - TS \tag{2.12}$$

where U is the internal energy of the system, T is the temperature and S is the entropy. The probability, *p*, assigned to a specific microstate in the canonical ensemble is subsequently given by:

$$p(\boldsymbol{r}^N \boldsymbol{p}^N) = e^{(F-E)/k_B T} = \frac{1}{Q} e^{-E/k_B T},$$
$$Q = e^{-F/k_B T} = \sum_i e^{-E_i/k_B T} \tag{2.13}$$

where E is the energy associated with the specific microstate of interest, k_B is the Boltzmann constant and Q is the canonical partition function. The index *i* in the summation runs over all possible microstates of the system within the canonical ensemble and each microstate is associated with a specific energy E_i. These equations show that the Helmholtz free energy intrinsically carries information

about the probability distribution of accessible microstates, while taking entropy effects explicitly into account. This renders *NVE* ensemble simulations extremely useful for predicting the internal dynamics of (bio-) molecular systems and materials. Equation (2.13) also plays an integral role in enhanced sampling simulations such as Metadynamics, or Blue Moon sampling, which are extensively used in chapter 4 of this thesis.[9–12] However, going into the details of these enhanced sampling methods is beyond the scope of this introduction. Chemical experiments are typically performed at constant pressure rather than constant volume. Hence, the driving force for chemical reactions is the gradient of the so-called Gibbs Free energy, which is defined as

$$G \equiv U + PV - TS = H - TS, \tag{2.14}$$

in which the pressure P and volume V term, together with the internal energy U sum to the enthalpy H. The main difference with the Helmholtz free energy is thus the inclusion of the PV term, which measures the work related to the volume change associated to the simulated phenomenon. Although this difference can be very important for studying phase transitions or other physical processes, the effect is rather small for most chemical conversions encountered in this thesis. As the critical MD simulations described in this dissertation are performed at constant volume, the terms *Helmholtz* and *Gibbs* free energies are used interchangeably.

A final point to address in this section on MD is how to deal with the finite size effects introduced by the boundaries of the simulation box. An effective way of avoiding finite size effects is to impose periodic boundary conditions (PBC). The idea behind PBC is that a periodic *image* of the unit cell is projected at all edges of the simulation cell, subsequently allowing particles to move through the boundary and re-appear on the other side of the box. Invoking periodic boundary conditions is associated with a neglectable computational cost, since each particle interacts only with the nearest image of all other particles in the system.

2.4 Excited States and Non-Adiabatic Dynamics

The previous discussion has focused on describing the nuclear dynamics of a molecular system in the electronic ground state. These simulations are interesting for a wide range of applications ranging from computation of thermodynamic quantities to probing the dynamics of ground state chemical reactions. However, in the context of solar-fuel production it is critical to investigate electronically excited states and explicitly calculate the coupling between nuclear and electronic degrees of freedom.

To describe excited state phenomena, we need to follow the time-evolution of the wavefunction as dictated by equation (2.1). The time-evolution of the electronic wavefunction is typically computed in terms of time-dependent wavefunction coefficients $c_i(t)$, in a basis of adiabatic eigenstates of the electronic Hamiltonian:

$$\Psi(\boldsymbol{r}, \boldsymbol{R}, t) = \sum_i c_i(t)\Psi_i(\boldsymbol{r}; \boldsymbol{R}; t) \,, \tag{2.15}$$

where $\Psi_i(\boldsymbol{r}; \boldsymbol{R}; t)$ are the eigenfunctions obtained from solving equation (2.4), and include a parametric time-dependence to account for the changing nuclear positions.[13] By inserting equation (2.15) into equation (2.1) and multiplying from the left by $\Psi_j^*(\boldsymbol{r};\ \boldsymbol{R}; t)$ we obtain:

$$\frac{\partial}{\partial t} c_j(t) = -\sum_i \left[iH_{ji} + T_{ji} \right] c_i \,, \tag{2.16}$$

where T_{ji} is the time-derivative coupling, calculated as $T_{ji} = \boldsymbol{v} \cdot \boldsymbol{d}_{ji}$, in which $\boldsymbol{v}$ collects all the nuclear velocities and $\boldsymbol{d}_{ji}$ is now a column vector containing the non-adiabatic coupling contributions for all nuclear coordinates (see equation (7)). In practice, the quantum chemistry method of choice can affect the nature of the basis states $\Psi_i(\boldsymbol{r}; \boldsymbol{R}; t)$ and the computation of $\boldsymbol{d}_{ji}$. For Time-Dependent DFT based approaches (see section 2.6.2), the basis states are generally not adiabatic, and the non-adiabatic couplings are either numerically intensive or analytically difficult to obtain. Therefore, the work discussed in this dissertation relies on a propagation scheme in which the eigen basis is obtained by diagonalizing the

Hamiltonian matrix at each time step, and the wavefunction coefficients are propagated based on the overlap matrix between subsequent time steps.[14,15]

Now that we have established a practical approach to evolve the quantum mechanical wavefunction coefficients for the electronic subsystem, the classical propagation of the nuclear coordinates can be discussed. One of the easiest approaches is to completely ignore electronic structure effects on the nuclear motion and simply evolve the nuclei on a potential energy surface generated by a single electronic eigenstate as described by equation (2.11). This approach is justifiable if the electronic motion is very fast compared to the nuclear response or if the nuclear response is generally negligible. Such scenarios are often encountered when studying interfacial electron or hole transfer processes in dye-semiconductor heterostructures. In Chapter 6 of this dissertation such a study is presented.

In many cases the nuclear response to the electronic wavefunction change cannot be ignored and needs to be considered explicitly. The main assumption in the Born-Oppenheimer approximation is that the classical motion of the nuclear subsystem is subject exclusively to a single potential energy surface generated by a single quantum mechanical electronic eigenstate $|j\rangle$. The main challenge thus lies in addressing situations where multiple electronic eigenstates contribute to the electronic wavefunction simultaneously. Historically, two approaches have been proposed to solve this problem. In the first approach, an averaged potential energy surface is defined in which all considered electronic states contribute according to their electronic wavefunction coefficient. This mean-field approach is referred to as the Ehrenfest method and captures the coherent motion between the nuclei and electrons naturally, while preserving a normalized wavefunction.[16] However, the mean-field character of this approach renders it impossible to describe trajectory-branching that occurs due to different trajectories being subject to different quantum states. This is specifically relevant when one is interested in a low probability channel that will never be accessed with the mean-field approach.[17]

With this issue in mind, John C. Tully developed an alternative method for simulating excited state molecular dynamics, which is now known as Fewest Switches Surface Hopping (FSSH).[2] The idea behind his approach is that instead of propagating a single trajectory on an averaged potential energy surface, an ensemble of trajectories is propagated on potential energy surfaces belonging to specific electronic eigenstates. The trick is to allow trajectories to "hop" between surfaces, based on a stochastic algorithm. In this way the population of trajectories subject to a specific quantum state remains approximately equal to the wavefunction amplitude associated with that state. Trajectories are allowed to switch to any coupled state at any point during the simulations, and the switching probability is governed by the quantum probabilities. The switching probability g_{ij}, for a trajectory to switch from state i to state j is calculated as:

$$g_{ij} = \frac{\Delta\tau \left[2\ \mathrm{Im}\left(c_j^* c_i\ H_{ji}\right) - 2\ \mathrm{Re}\left(c_j^* c_i\ \boldsymbol{R}\cdot\boldsymbol{d}_{ji}\right)\right]}{c_j c_j^*}. \tag{2.17}$$

where $\Delta\tau$ is the time step at which the electronic subsystem is propagated. In most surface hopping implementations, the electronic subsystem is propagated with a time step at least one order of magnitude smaller than the classical time step Δt. For a trajectory in active state $|\lambda\rangle$, the hopping probabilities $g_{\lambda j}$ are calculated at each quantum time step $\Delta\tau$. Transition probabilities lower than zero are set to zero. This minimizes the number of hops, hence *Fewest Switches*. Subsequently, a random number ζ is drawn between 0 and 1. At each quantum time step, the following equation is evaluated for all states $|k\rangle$:

$$\sum_{j=1}^{k-1} g_{\lambda j} < \zeta < \sum_{j=1}^{k} g_{\lambda j} \tag{2.18}$$

If the equation holds for any state $|k\rangle$, then a hop to potential energy surface E_k is attempted at the next classical time step. Once a state is found for which equation (2.18) is satisfied, no further hopping attempts are undertaken until the new time step $t + \Delta t$ is reached. Figure 2.1 presents a schematic overview of the FSSH algorithm.

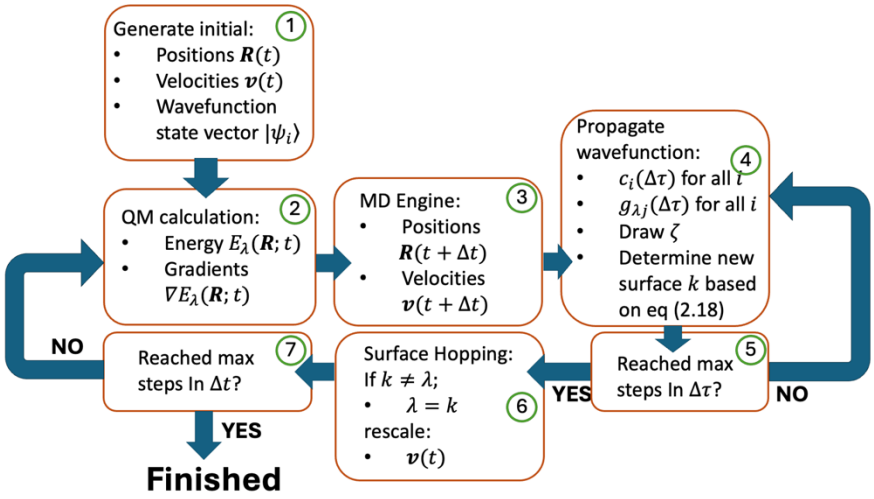

Figure 2.1. Schematic overview of the typical FSSH algorithm.

Analogous to ground state MD simulations, the first step in a FSSH simulation requires generating a set of initial positions and velocities. Additionally, FSSH also requires preparation of an initial electronic state vector. Here one may choose to initiate the wavefunction in a specific electronic eigenstate, or one can calculate explicitly the wavefunction coefficients based on the interaction of a molecule with an external electromagnetic field. Steps 2 and 3 in Figure 2.1 do not deviate from a normal MD scheme, except for the fact that the energies and gradients are not only calculated for the ground state but also for one or more excited states. The exact number of required gradients depends on the decoherence correction schemes.[18] In step 4, the newly obtained positions and velocities are used to evolve the electronic wavefunction. At each new sub-time step $\tau + \Delta\tau$, the hopping probabilities to all states are evaluated using equation (2.17). Then, a random number ζ is draw, and the label k is saved for which equation (2.18) holds. A hop to the new state is invoked in step 6, after the electronic wavefunction propagation is finished. The change in potential energy in the system is adjusted for by scaling the nuclear velocities such that the sum of potential and kinetic energies remains constant. Finally, the trajectory is truncated after a desired

simulation time has been reached, or the algorithm goes back to step 2.

One of the most prominent issues with the FSSH is that the coherences between different electronic eigenstates are insufficiently damped. Because the nuclear motion is subject only to a single electronic energy surface, wavefunction branching due to diverging nuclear trajectories is not captured. In the past three decades a range of hopping algorithms have been derived which try to address this issue.[18–20] Recently, a pedagogical paper on FSSH was published that discusses the issue of decoherence in an intuitive manner.[21]

2.5 Obtaining Thermodynamic Properties from Static Calculations

Although molecular dynamics is an elegant way of including solvent and entropy effects explicitly into the computational study of chemical reactions, the associated computational cost is often a limiting factor when high accuracy in the interatomic potentials is required. In such cases it is common practice to consider only the molecule of interest in its minimal potential energy structure without explicit solvent molecules. The assumption is that the potential energy minimum is representative for the average structure of the molecule, which in many cases is reasonable especially for relatively rigid systems. Solvent and thermodynamic effects can subsequently be added a posteriori using a few simple approximations. The internal energy U can be approximated as the sum of the electronic energy E_{scf} and the nuclear internal energy E_{NI}, which in turn is partitioned in translational, rotational and vibrational contributions. The first two contributions can easily be shown to amount to $\frac{3}{2}\,k_{\mathrm{B}}T$, where each translational and rotational degree of freedom contributes $\frac{1}{2}\,k_{\mathrm{B}}T$. The vibrational zero-point energy is

$$E_{\mathrm{ZP}} = R\sum_{j}^{3N-6} v_j\left(\frac{1}{2}+\frac{1}{(e^{v_j/T}-1)}\right), \tag{2.19}$$

where v_j is the angular frequency of the j'th eigenmode, $3N-6$ is the number of vibrational modes for a non-linear molecule and R is the gas constant.[22] The

internal vibrations are calculated as the eigenvectors of the Hessian within the harmonic approximation. The vibrational entropy is calculated as:

$$S_v = R \sum_{j}^{3N-6} \left[\frac{v_j/T}{\left(e^{v_j/T} - 1\right)} - \ln(1 - e^{-v_j/T}) \right], \tag{2.20}$$

where the low frequency modes are often scaled down to reduce numerical noise which may become large due to the first term on the right hand side of the equation.[23,24] In addition, small corrections might be imposed to account for thermal occupation of vibrational excited states. Finally, the PV contribution in equation (2.14) can be approximated by the ideal gas law, *i.e.* $PV = NRT$. Solvent corrections may be calculated completely a posteriori or may be considered during the geometry optimization and frequency calculations. However, the studies in this dissertation, and specifically chapter 5, use optimizations in the gas phase. Therefore, the solvation term, ΔG^0_{solv}, covers the solvation energy associated with moving from the gas phase to the solution phase. This term is calculated with implicit continuous solvation models such as COSMO, or SMD.[25–27] The Gibbs free energy of a molecule in solution, $G^0(\text{solv})$, is calculated as:

$$G^0(\text{solv}) = E_{\text{scf}}\,(\text{gas}) + E_{NI}\,(\text{gas}) - TS\,(\text{gas}) + \Delta G^0_{\text{solv}} + \Delta G^{0/*} \tag{2.21}$$

Here, the $E_{\text{scf}}\,(\text{gas})$ contribution is taken as the energy obtained from the electronic structure theory calculation and the $E_{NI}\,(\text{gas})$ variable is the sum of the E_{ZP}, translational and rotational internal energy contributions. The $\Delta G^{0/*}$ contribution quantifies the Gibbs free energy difference related to changing from standard state conditions (1 Atm in the gas phase) to the desired concentration in solution. For a chemical reaction in solution, this term is calculated as:

$$\Delta G^{0/*} = RT\ln(24.46 * [molecule]) \tag{2.22}$$

where $[molecule]$ is the molecular concentration.[28] Having the flexibility to easily take into account concentration differences is a big advantage of this *static* approach, especially when dealing with reactions that are driven by Chatelier's principle such as ligands that coordinate to metal complexes or protonation

reactions. However, disadvantages of the static approach arise when the solvent interactions need to be sampled explicitly or when anharmonic terms dominate the vibrational spectrum.

2.6 Electronic Structure Methods

2.6.1 Density Functional Theory

The previous sections have focused on describing the mixed quantum-classical dynamics of atomic nuclei on the electronic potential energy surfaces, without explicitly addressing how the stationary Schrödinger equation is solved. We now shift our attention to finding solutions to the electronic structure problem stated in equation (2.4). In the past three decades, density functional theory (DFT) has established itself as the workhorse of quantum chemical calculations, because of its reasonable accuracy and limited numerical cost. Given the wealth of books and review papers available on the theory and application of DFT, we will focus here strictly on the fundamental concepts.[29–32]

The foundation for DFT was laid in 1964 by Hohenberg and Kohn,[33] who showed that the ground state energy of an inhomogeneous interacting electron gas, subject to an external potential $v(\boldsymbol{r})$,

$$E[\rho] = \int_{\mathbb{R}^3} d\boldsymbol{r}\, v(\boldsymbol{r})\rho(\boldsymbol{r}) + \frac{1}{2}\int_{\mathbb{R}^3} d\boldsymbol{r}\, d\boldsymbol{r}' \frac{\rho(\boldsymbol{r})\rho(\boldsymbol{r}')}{|\boldsymbol{r}-\boldsymbol{r}'|} + G[\rho], \tag{2.23}$$

is a unique functional of the electronic density $\rho(\boldsymbol{r})$. Here, $\mathbb{R}^3$ signifies the integral over all real space. The first term in this equation covers the interaction of the electronic system with the external potential, while the second term represents the coulomb energy. The functional $G[\rho]$ is defined as the difference between the exact density functional and the first two terms. It is important to note that $G[\rho]$ depends uniquely on the density ρ and not on the external potential $v(\boldsymbol{r})$. Hohenberg and Kohn demonstrated that inserting the true electron density $\rho(\boldsymbol{r})$ into equation (2.23) yields an absolute minimum for $E[\rho]$, corresponding to the system's ground state. This implies that the ground state energy E_{GS} can be found

by minimization of the energy functional with respect to the density

$$E_{\mathrm{GS}} = \min_{\rho} E[\rho] \,, \tag{2.24}$$

subject to the constraint that the total density integral is conserved, thus ensuring conservation of particle number. Soon after publication of the Hohenberg Kohn theorem, Kohn and Sham introduced a practical approximation to $G[\rho]$, which allowed them to derive a set of self-consistent equations that can be used to perform calculations on chemically relevant systems.[34] They first separated $G[\rho]$ into two parts:

$$G[\rho] \equiv T_{\mathrm{s}}[\rho] + E_{\mathrm{xc}}[\rho] \tag{2.25}$$

where $T_{\mathrm{s}}[\rho]$ represents the electronic kinetic energy and $E_{\mathrm{xc}}[\rho]$ represents the so-called exchange-correlation (XC) functional. The key insight now lies in recognizing that the true electron density of the system can be expressed in terms of a set of fictitious non-interacting electrons. The density of this fictitious system is described as a sum of squared single-particle wavefunctions according to

$$\rho\,(\boldsymbol{r}) = 2\sum_{i=1}^{n/2} |\varphi_i(\boldsymbol{r})|^2 \,. \tag{2.26}$$

Here n is the number of electrons and the factor 2 accounts for the double occupancy of each spatial orbital $\varphi_i(\boldsymbol{r})$, assuming a closed shell spin configuration. The single-particle spatial orbitals are constrained to remain orthonormal. Equation (2.26) simplifies the evaluation of the electronic kinetic energy functional, allowing equation (2.23) to be written as

$$E[\rho] = \int_{\mathbb{R}^3} d\boldsymbol{r}\; v(\boldsymbol{r})\rho(\boldsymbol{r}) + \frac{1}{2}\int_{\mathbb{R}^3} d\boldsymbol{r}\; d\boldsymbol{r}'\,\frac{\rho(\boldsymbol{r})\rho(\boldsymbol{r}')}{|\boldsymbol{r}-\boldsymbol{r}'|} + 2\sum_{i=1}^{N/2}\left\langle \varphi_i(\boldsymbol{r})\middle| -\frac{1}{2}\nabla^2 \middle|\varphi_i(\boldsymbol{r})\right\rangle + E_{\mathrm{xc}}[\rho] \,. \tag{2.27}$$

Kohn and Sham showed that, by minimizing this functional with respect to the density, one can obtain a set of single particle eigenvalue equations

$$\left\{-\frac{1}{2}\nabla^2 + v(\boldsymbol{r}) + \int_{\mathbb{R}^3} \frac{\rho(\boldsymbol{r}')}{|\boldsymbol{r}-\boldsymbol{r}'|} d\boldsymbol{r}' + v_{\mathrm{xc}}(\boldsymbol{r})\right\}\varphi_i(\boldsymbol{r}) = \varepsilon_i \varphi_i(\boldsymbol{r}) \tag{2.28}$$

that can be solved in a self-consistent manner. The $v_{\mathrm{xc}}(r) = \delta(E_{\mathrm{xc}}(r))/\delta\rho$ is the XC potential, and the ε_i are the Kohn-Sham energy eigenvalues. In theory, equation (2.28) is exact within the Born-Oppenheimer approximation. However, in practice the exact XC potential for any practically useful system is unknown. Finding numerically tractable and physically accurate approximations to $v_{\mathrm{xc}}(r)$ is an active research area and a very large number of functionals have been proposed.[35]

The first XC functional, introduced by Kohn and Sham in their seminal paper, is now known as the Local Density Approximation (LDA).[34] They derived the exact functional for the XC energy of a uniform electron gas (UEG) and used this functional to approximate the XC energy density of the inhomogeneous system under study. The XC energy with the LDA approximation is thus calculated as

$$E_{\mathrm{xc}}^{\mathrm{LDA}}[\rho] = \int_{\mathbb{R}^3} e_{\mathrm{xc}}^{\mathrm{UEG}}\big(\rho(\boldsymbol{r})\big)\rho(\boldsymbol{r})d\boldsymbol{r}\,, \tag{2.29}$$

where $e_{\mathrm{xc}}^{\mathrm{UEG}}(\rho)$ is a functional that returns for any given density the energy per particle of the UEG with that density.

Although the LDA approximation yields reasonable results for specific problems in solid state physics, its generally not accurate enough to study properties of molecular systems. A considerable improvement over LDA-DFT can be achieved with generalized gradient approximations (GGA) that consider explicitly the local gradient of the electron density. Later, meta-GGA functionals have been proposed that account also for the Laplacian of the density and hybrid-functionals were developed that incorporate an empirically determined fraction of exact Hartree-Fock exchange (HFX) into the XC potential. While GGA-functionals are generally effective at producing accurate bonding energies and molecular structures, they suffer from a large delocalization error due to self-interaction of

the electronic density.[36] Consequently, transition states and band gaps are underestimated and charge tends to be over-delocalized. Chapter 4 of this dissertation assesses how the inclusion of HFX affects the localization of spin densities in DFT-based MD simulations of a supramolecular water oxidation catalyst-dye complex.

2.6.2 Time-Dependent Density Functional Theory

The Hohenberg-Kohn theorem proves that the external potential $v(\boldsymbol{r})$ uniquely determines the ground state electron density distribution $\rho\ (\boldsymbol{r})$ of a many-body system, and that the ground state wavefunction is a unique functional of $\rho\ (\boldsymbol{r})$.[33] This implies that any ground state property of interest can be calculated as a functional of the ground state density. However, as mentioned before, we are also interested in properties of molecules in electronically excited states. In 1984, Runge and Gross demonstrated that a similar unique mapping exists between the time-dependent density of a many-body system subject to a time-dependent potential $v(\boldsymbol{r}, t)$.[37] This theory provides a formal basis extending the application of DFT to the calculation of excited state properties, and nowadays, linear response time-dependent DFT (LR-TDDFT) has become one of the most popular methods of choice to calculate optical properties in molecules.[38] The main idea is to calculate the first order density response $\delta\rho$ to a small change in $v(\boldsymbol{r}, t)$ in a basis of fully converged ground state Kohn-Sham orbitals. A more elaborate derivation of LR-TDDFT can be found in literature.[39] As we are interested in excitation energies, the response function is calculated in the frequency (ω) domain:

$$\delta\rho(\boldsymbol{r}, \omega) = \int_{\mathbb{R}^3} \chi(\boldsymbol{r}, \boldsymbol{r}';\ \omega)\delta v_{\text{eff}}(\boldsymbol{r}', \omega)\, d\boldsymbol{r}'. \tag{2.30}$$

Here, $\chi(\boldsymbol{r}, \boldsymbol{r}';\ \omega)$ is the response function, which can be expressed in terms of occupied (φ_i) and virtual (φ_a) Kohn-Sham orbitals and energy eigenvalues:

$$\chi(\boldsymbol{r},\boldsymbol{r}';\,\omega) = \sum_{i=1}^{\frac{n}{2}}\sum_{a=1}^{\frac{m}{2}} 2\frac{\omega_{ai}}{\omega-\omega_{ai}}\varphi_i(\boldsymbol{r})\varphi_{ja}(\boldsymbol{r})\varphi_i(\boldsymbol{r}')\varphi_{ja}(\boldsymbol{r}'), \tag{2.31}$$

where n is the number of occupied spatial orbitals, m the number of empty spatial orbitals, and $\omega_{ai} \equiv \varepsilon_a - \varepsilon_i$ is the difference of Kohn-Sham energies between state i and a. The perturbation in the effective potential is

$$\delta v_{\text{eff}}(\boldsymbol{r}',\omega) = \delta v(\boldsymbol{r},\omega) + \int_{\mathbb{R}^3}\frac{\delta\rho(\boldsymbol{r}',\omega)}{|\boldsymbol{r}-\boldsymbol{r}'|}d\boldsymbol{r}' + \int_{\mathbb{R}^3}\delta f_{\text{xc}}(\boldsymbol{r},\boldsymbol{r}';\,\omega)\delta\rho(\boldsymbol{r},\omega)d\boldsymbol{r}'\,. \tag{2.32}$$

The first and second term on the right-hand side of the equation represent the perturbation in the external potential and the electronic density, respectively. The third term contains the time-dependent XC kernel

$$\delta f_{\text{xc}}(\boldsymbol{r},\boldsymbol{r}';\,\omega) = \left.\frac{\delta v_{\text{xc}}(\boldsymbol{r},\omega)}{\delta\rho(\boldsymbol{r}',\omega)}\right|_{\rho=\rho_0}. \tag{2.33}$$

Here the functional derivative is taken with respect to the ground state density. Analogous to the XC potential in ground state DFT, the XC kernel in linear response TDDFT needs to be approximated. In practice, the Adiabatic Local Density Approximation (ALDA) is commonly applied, and it is also the approximation of choice in this dissertation.[40]

2.7 References

[1] N. L. Doltsinis, D. Marx, *J. Theor. Comput. Chem.* **2002**, *01*, 319–349.
[2] J. C. Tully, *J. Chem. Phys.* **1990**, *93*, 1061–1071.
[3] P. A. M. Dirac, *Math. Proc. Camb. Phil. Soc.* **1939**, *35*, 416–418.
[4] W. C. Swope, H. C. Andersen, P. H. Berens, K. R. Wilson, *J. Chem. Phys.* **1982**, *76*, 637–649.
[5] A. Torres, R. S. Oliboni, L. G. C. Rego, *J. Phys. Chem. Lett.* **2015**.
[6] S. Nosé, *J. Chem. Phys.* **1984**, *81*, 511–519.
[7] W. G. Hoover, *Phys. Rev. A* **1985**, *31*, 1695–1697.
[8] G. Bussi, D. Donadio, M. Parrinello, *J. Chem. Phys.* **2007**, *126*, 014101.
[9] A. Laio, F. L. Gervasio, *Rep. Prog. Phys.* **2008**, *71*, 12660.
[10] A. Barducci, M. Bonomi, M. Parrinello, *Wiley Interdiscip. Rev. Comput. Mol. Sci.* **2011**, *1*, 826–843.
[11] G. Bussi, A. Laio, *Nat. Rev. Phys.* **2020**, *2*, 200–212.
[12] G. Ciccotti, M. Ferrario, *Mol. Simul.* **2004**, *30*, 787–793.

[13] S. Mai, P. Marquetand, L. González, *WIREs Comput Mol Sci.* **2018**, *8*, e1370.
[14] S. Mai, P. Marquetand, L. González, *Int. J. Quantum Chem.* **2015**, *115*, 1215–1231.
[15] G. Granucci, M. Persico, A. Toniolo, *J. Chem. Phys.* **2001**, *114*, 10608–10615.
[16] S. Choi, J. Vaníček, *J. Chem. Phys.* **2021**, *155*, 124104.
[17] J. C. Tully, *Faraday Discuss.* **1998**, *110*, 407–419.
[18] A. Jain, E. Alguire, J. E. Subotnik, *J. Chem. Theory Comput.* **2016**, *12*, 5256–5268.
[19] H. M. Jaeger, S. Fischer, O. V. Prezhdo, *J. Chem. Phys.* **2012**, *137*, 22A545.
[20] J. E. Subotnik, N. Shenvi, *J. Chem. Phys.* **2011**, *134*, 30–45.
[21] A. Jain, A. Sindhu, *ACS Omega* **2022**, *7*, 45810–45824.
[22] J. W. Ochterski, "Thermochemistry in Gaussian", 2000, Gaussian, Inc., 1-19, June 2, 2000.
[23] S. Grimme, ***Chem. - Eur. J.*** **2012**, *18*, 9955–9964.
[24] Y.-P. Li, J. Gomes, S. Mallikarjun Sharada, A. T. Bell, M. Head-Gordon, *J. Phys. Chem. C* **2015**, *119*, 1840–1850.
[25] A. Klamt, *J. Phys. Chem.* **1995**, *99*, 2224–2235.
[26] A. Klamt, V. Jonas, *J. Chem. Phys.* **1996**, *105*, 9972–9981.
[27] A. V. Marenich, C. J. Cramer, D. G. Truhlar, *J. Phys. Chem. B* **2009**, *113*, 6378–6396.
[28] C. P. Kelly, C. J. Cramer, D. G. Truhlar,*J. Phys. Chem. B* **2006**, *110*, 16066–16081.
[29] E. Cancès, G. Friesecke, Eds. , *Density Functional Theory: Modeling, Mathematical Analysis, Computational Methods, and Applications*, Springer International Publishing, Cham, **2023**.
[30] N. Argaman, G. Makov, *Am. J. Phys.* **2000**, *68*, 69–79.
[31] R. Car, *Quant. Struct.-Act.Relat.* **2002**, *21*, 97–104.
[32] M. Orio, D. A. Pantazis, F. Neese, *Photosynth. Res.* **2009**, *102*, 443–453.
[33] P. Hohenberg, W. Kohn, *Phys. Rev.* **1964**, *136*, B864–B871.
[34] W. Kohn, L. J. Sham, *Phys. Rev.* **1965**, *140*, A1133–A1138.
[35] N. Mardirossian, M. Head-Gordon, *Mol. Phys.* **2017**, *115*, 2315–2372.
[36] K. R. Bryenton, A. A. Adeleke, S. G. Dale, E. R. Johnson, *WIREs Comput. Mol. Sci.* **2023**, *13*, e1631.
[37] E. Runge, E. K. U. Gross, *Phys. Rev. Lett.* **1984**, *52*, 997–1000.
[38] C. Adamo, D. Jacquemin, *Chem. Soc. Rev.* **2013**, *42*, 845–856.
[39] C. A. Ullrich, *Time-Dependent Density-Functional Theory: Concepts and Applications*, Oxford University Press, **2011**.
[40] S. J. A. Van Gisbergen, J. G. Snijders, E. J. Baerends, *J. Chem. Phys.* **1995**, *103*, 9347–9354.